

ORIGINAL RESEARCH

Open Access



Three dimensional BC/rGA aerogel: preparation, characterization, and adsorption of Cr(VI)

Naiju Che, Na Liu, Yinhui Li, Chao Li, Yanli Liu* and Chengliang Li* 

Abstract

Graphene-based composite aerogel doped with other low-cost materials can reduce the cost and promote the use in water treatment. This work prepared ball-milled biochar/reduced graphene oxide aerogel (BC/rGA) using GO and low-cost ball-milled biochar (BC) in a certain proportion with the freeze-thawing technique and sol-gel method, and applied BC/rGA on the Cr(VI) removal from aquatic environments. The characterization results showed that aerogel had a honeycomb briquette three-dimension (3D) and mesoporous structure with interconnected pores, and proved the preparation progress of aerogel in principle. Compared with GO, rGA and BC/rGA had better adsorption performance with 3D structure and well-developed pores, and BC/rGA with the mixture ratio of BC and GO of 1:4 was more appropriate. The adsorption kinetics data of rGA and BC/rGA_(1:4) were fitting well with the pseudo-second-order model ($R^2 > 0.951$), and the isotherm adsorption results were fitting the Langmuir model well ($R^2 > 0.974$). The results demonstrated that the adsorption process was monolayer and endothermic adsorption involving chemisorption. Additionally, the adsorption capacities of rGA and BC/rGA_(1:4) at solution pH 2 were 3.71 and 3.89 times greater than those at solution pH 8, respectively. High background ion strength and low temperature slightly inhibited the adsorption of Cr(VI) by both rGA and BC/rGA_(1:4). The adsorption mechanisms of Cr(VI) on rGA and BC/rGA_(1:4) were electrostatic interaction, reduction and ion exchange. The use of BC/rGA could reduce the cost and promote the green reuse of agricultural waste. Overall, BC/rGA could be used as a promising green adsorbent alternative for the feasible treatment of heavy metal contaminated water.

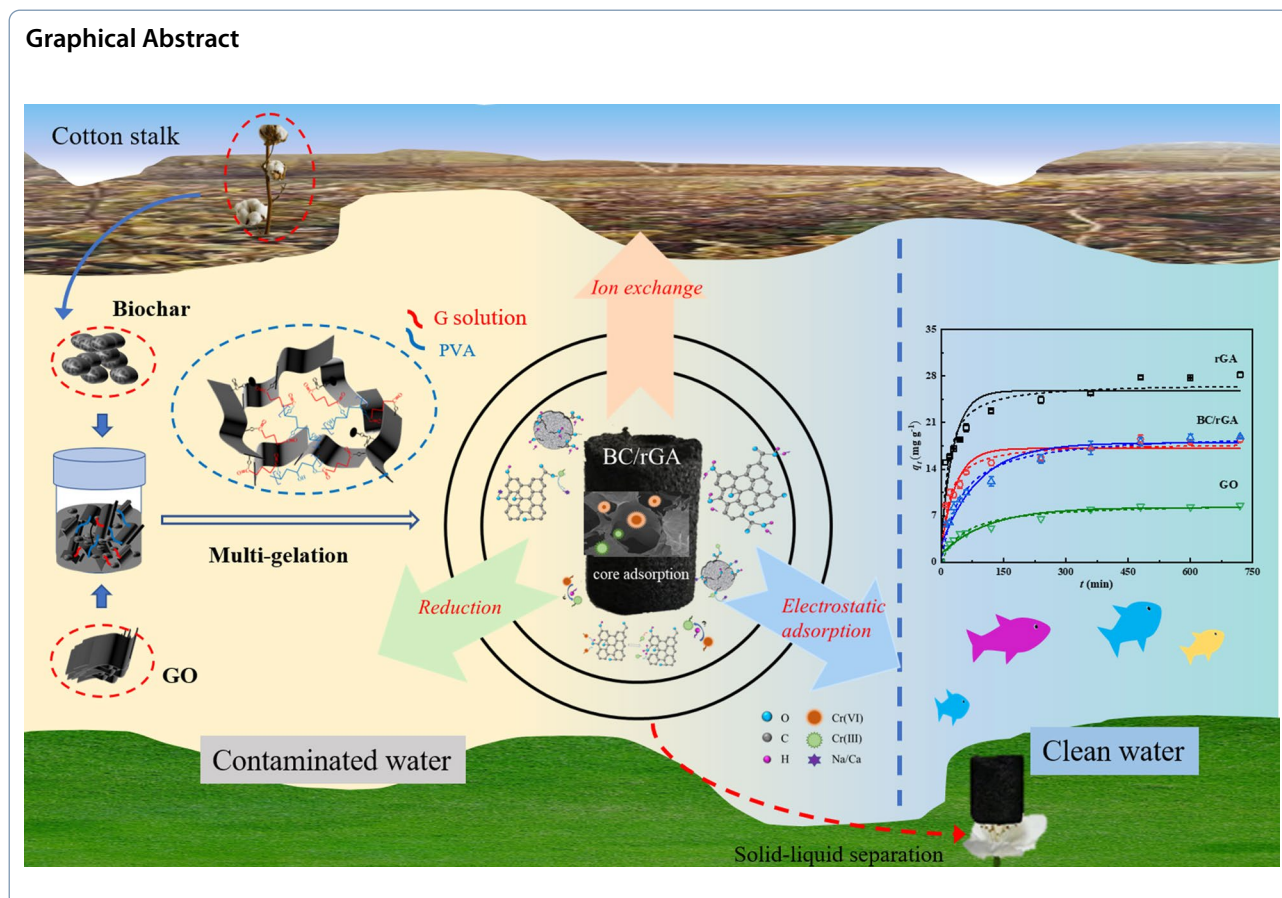
Highlights

- Ball-milled biochar/reduced graphene oxide aerogel (BC/rGA) could reduce the cost and cumbersome preparation steps of aerogel.
- BC/rGA had a honeycomb briquette three-dimension (3D) structure with interconnected pores and could directly be separated from solution.
- BC/rGA had 2.23 times of Cr(VI) adsorption capacity higher than GO and the adsorption was obviously affected by solution pH.

Keywords: Graphene aerogel, Ball-milled biochar, Heavy metal, Adsorption mechanism

*Correspondence: yanliliu2013@163.com; chengliang_li11@163.com

National Engineering Research Center for Efficient Utilization of Soil and Fertilizer Resources, College of Resources and Environment, Shandong Agricultural University, Tai'An 271018, China



1 Introduction

Chromium (Cr) is a common heavy metal ion with high toxicity and causes serious negative impacts on human health when the concentration exceeds the standard limits (Joseph et al. 2019; Shaheen et al. 2022; Zhitkovich 2011). The permissible limit of total Cr analyzed by World Health Organization (WHO) is 0.05 mg L^{-1} , and the limit from Environmental Protection Agency (EPA) is 0.1 mg L^{-1} (Liu et al. 2019; Wang et al. 2017c). However, Cr-contaminated water is still discharged into natural environment every year, even under the treatment. Many industrial processes have generated Cr-contaminated water including electroplating, leather tanning, nuclear power plant and etc. (Wang et al. 2015). Because Cr(VI) takes on the great toxicity, which has teratogenicity, mutagenicity and carcinogenicity (Mo et al. 2019), the removal/reduce of Cr(VI) from contaminated water has been studied (Behnajady and Bimeghdar 2014; Tang et al. 2021) and is still considered to be of urgency. Adsorption has shown superior to other methods in contaminated water treatment due to its low cost, low energy and high efficiency, including Cr(VI) removing/reducing (Li et al. 2017; Yu et al. 2020).

Aerogels are considered to be one of ideal adsorbents for contaminated water treatment with low density and abundant functional groups (Mei et al. 2020), which have a porous solid network and can be separated directly and recovered easily compared with powder adsorbents (Hasanpour and Hatami 2020). Graphene oxide (GO) has been regarded as one of the innovative materials for the synthesis of aerogels due to its chemical stability and abundant functional groups (Korkmaz and Kariper 2020; Wei et al. 2020), and the research of graphene aerogels has dramatically increased since the first report in 2009 (Korkmaz and Kariper 2020), including the synthesis, modification and application (Wang et al. 2020). So far, graphene aerogels have been fabricated via various methods including chemical vapor deposition, template mediated assembly, 3D printing, hydrothermal process, and freeze-casting strategy (Additional file 1: Table S1). However, some of these methods are complicated, and reducing reagent are highly toxic, strongly corrosive and explosive, even the volume contraction of the prepared aerogel is serious (Lee and Park 2020; Shang et al. 2020). In the last decades, reduced graphene oxide aerogel (rGA) has

been widely used in energy storage (Serrapede et al. 2019), sensors (Li and Wang 2020), catalysts (Zhao et al. 2019) and so on. Although rGA has excellent pore structure and large surface area (Wei et al. 2020) which are in favor of adsorption, rGA has not widely applied in removing heavy metals from contaminated water in treatment plant with the high cost and complex preparation steps. A large number of studies have been devoted to the preparation of graphene-based composite aerogel by adding other materials on the basis of preserving the advantages of GO in recent years, and the common additive materials are chitosan (Wang et al. 2021), polymers (Wang et al. 2017b; Ye et al. 2017), carbon nanotubes (Wang et al. 2017a), minerals (Zhang et al. 2018), biochar (Wei et al. 2020), and etc. Along this line, a preparation method with simple procedure, no secondary contamination and low cost additive materials should be selected for the preparation of graphene-based composite aerogel.

Biochar is a kind of carbon-rich solid material with ample micropore structure (Sakhiya et al. 2020), which is obtained from the pyrolysis or hydrothermal carbonization of raw biomass under oxygen-limited or oxygen-free conditions (Kołtowski et al. 2017), and has carbon sequestration function to mitigate climate change (Li et al. 2018; Liu et al. 2013) and indirectly supports waste management (Qiu et al. 2022). Biochar can be produced from various agricultural and industrial wastes (Dai et al. 2021; Liu et al. 2020; Pradhan et al. 2020), and the use of biochar will promote the reuse of resources and be in line with the direction of sustainable development. Thus, biochar could be regarded as a sustainable, carbon-neutral material (Yuan et al. 2019). Because of the features of low cost, large specific surface area (SSA), abundant oxygen-containing functional groups and redox properties (Hu et al. 2020; Leng et al. 2021; Pradhan et al. 2020), biochar has played an important role in the adsorption of heavy metals (Gupta et al. 2020; Shaheen et al. 2022), including Pb (Xiong et al. 2021), Sb (Chen et al. 2022), Cr (Zou et al. 2021), Cu (Xiao et al. 2020), Cd (Liu et al. 2021a, b) and so on. However, as a powder adsorbent, the application of BC or BC-based composites inevitably releases particles into water and the general separation method from solution is filtration or centrifugation, by which it is difficult to separate and recycle biochar from the solution and might cause further biological toxicity and energy loss (Liang et al. 2021; Lu et al. 2020; Zhang et al. 2019).

Based on all the above studies, this study hypothesized that ball-milled biochar/reduced graphene oxide aerogel (BC/rGA) could comprehensively utilize the advantages of GO and BC (obtained from cotton stalk) to overcome the shortcomings of single-component materials. This

work will provide a simple and environmentally-friendly approach for preparing BC/rGA with different mass proportion of BC and rGO, comparatively analyze the characterization and adsorption capacity, and investigate the adsorption behavior of Cr(VI) on BC/rGA under different environmental conditions (solution pH, temperature, and ionic strength of background solution). This method could avoid the expensive raw materials and cumbersome steps of prior methods, such as solvent exchange and supercritical drying. The ultimate goal is to promote the utilization of waste resources and develop the application of GO based aerogel in environmental pollution control.

2 Materials and methods

2.1 Materials and chemicals

Raw graphite was purchased from Qingdao Nanshu Ruiying Graphite Co. Ltd. (Shandong, China). Cotton stalk was collected from farmland (Shandong, China). Poly vinyl alcohol (PVA) (with the degree of polymerization of 1700 and the alcoholysis degree of 98–99%) was purchased from Aladdin Industrial Corporation (Shanghai, China).

All the other chemicals and reagents used (including acetic acid, sulfuric acid, sodium hydrate, etc.) were of analytical grade without further purification and were purchased from Kaitong Chemical Reagent Co. Ltd. (Tianjin, China).

2.2 Adsorbent preparation

2.2.1 Preparation of GO and BC

GO was prepared from graphite according to a modified Hummer's method (Yang et al. 2015; Liu et al. 2021a, b) and BC was prepared from cotton stalk (Shandong, China). The cotton stalk was repeatedly washed with deionized water to remove impurities and dried at 80 °C in an oven. Then the dry cotton stalk was sieved to 2 mm particles by a grinder. After that, the porcelain boats with cotton stalk powder were put in a tube furnace and heated to 500 °C at a heating rate of 15 °C min⁻¹ for 2 h under the flow of nitrogen. The obtained biochar and steel ball were placed in an agate tank and ball milled at the speed of 300 rpm for 6 h using the planetary ball milling machine (Focucy, F-P2000, China).

2.2.2 Preparation of rGA and BC/rGA

The details of reagent preparation are shown in the Additional file 1 (SI. 1) and the aerogels were prepared on the basis of the preliminary test (Additional file 1: SI. 2). Firstly, 60 mL 5 mg L⁻¹ GO and BC/GO (the mass ratio of BC to GO was 1:10, 1:4, and 1:2, respectively) solution was prepared, respectively. Then, 3 mL 100 mg L⁻¹ PVA solution and 10 mL glutaraldehyde mixed solution were put into the GO or BC/GO solution under stirring.

The mixture was poured into a container and had five cycles of freezing–thawing. After that, the sample was immersed into L-ascorbic acid solution for 12 h at 80 °C to reduce the GO and then washed by 75% alcohol solution to removal the residual reagents. Finally, the samples were freeze-dried at -50 °C for 48 h, and the aerogels were obtained (Additional file 1: Fig. S3) which were named rGA, BC/rGA_(1:10), BC/rGA_(1:4), and BC/rGA_(1:2), respectively. On account of the poor mechanical stability, BC/rGA_(1:2) was easy to be broken, so it was not suitable for subsequent adsorption experiments.

2.3 Characterization methods

The morphology of tested materials was observed on a scanning electron microscope (SEM) (SU8020, Hitachi Limited, Japan) and Transmission Electron Microscope (TEM) (FEI Tecnai G2 F30, FEI, USA). The structure and composition analyses were conducted using N₂ adsorption–desorption isothermal test (ASAP 2460, micromeritics, USA) with Barrett–Joyner–Halender (BJH) method, Raman Spectrometer (Renishaw inVia, Renishaw, UK), X-ray diffractometer (XRD) (D8 Advance, Bruker, Germany), Fourier transform infrared (FTIR) (Nicolet 6700, Thermo Fisher Scientific, USA) and X-ray photoelectron spectroscopy (XPS) (Thermo Escalab 250 Xi, Thermo Fisher Scientific, USA).

2.4 Experiments for the adsorption of Cr(VI)

Batch adsorption experiments were conducted to investigate the adsorption mechanism of Cr(VI) on GO, rGA and BC/rGA, and the effect of environmental factors on Cr(VI) adsorption. 500 mg L⁻¹ Cr(VI) solution (pH 2.0) was prepared by dissolving K₂Cr₂O₇ in 0.01 M NaCl solution (pH 2.0), and the solution was diluted to the appropriate concentration using background electrolyte. All the batch adsorption experiments were conducted in triplicate with the adsorbent dose of 1 g L⁻¹, and the mixed solution was shaken in a constant temperature oscillating machine at 150 rpm. After the adsorption, solid–liquid separation was achieved by filtrating with membrane for GO and directly taking out for aerogels, respectively (Additional file 1: Fig. S4). The Cr(VI) concentration of solution was detected by atomic absorption spectrophotometer (PinA Aclé 900F, PerkinElmer Inc, USA).

The adsorption kinetics of GO, rGA and BC/rGA for Cr(VI) were studied by immersing 10 mg GO or aerogels into 10 mL 50 mg L⁻¹ Cr(VI) solution (pH 2.0) and the data were collected at specific times (0, 10, 20, 30, 45, 60, 120, 240, 360, 480, 600, 720 min) at room temperature (298 K). Adsorption isotherm parameters were determined by performing experiments at 298 K (shaking time was 12 h), and using Cr(VI) solutions with different

initial concentrations (10, 20, 40, 50, 60, 80, 100 mg L⁻¹, pH=2.0). After the adsorption experiment with 50 mg L⁻¹ Cr(VI) at pH 2.0 reached equilibrium, aerogels were put into 0.1 M H₂SO₄ solution and shaken for 12 h at 150 rpm and room temperature. And then the aerogels were washed with DI water several times until the pH value of effluent was nearly 7. The aerogels were used for the next cyclic adsorption after drying. Effects of solution pH, background electrolyte and temperature on Cr(VI) adsorption process were investigated under the same conditions (initial Cr(VI) solution concentration was 50 mg L⁻¹, and shaking time was 12 h). The pH value of solutions was set to 2.0, 4.0, 6.0, 8.0 and 10.0 with a background electrolyte of 0.01 M NaCl at 298 K. The background electrolyte was divided into ion type (0.01 M NaCl, 0.01 M CaCl₂) and ion intensity (0.01 M, 0.05 M, 0.1 M, 0.15 M, 0.2 M) with with a PH of 2.0 and a temperature of 298 K. The temperature was set to 288, 298 and 303 K for the adsorption isotherm experiments.

2.5 Data analysis

The adsorption capacity calculation formula, adsorption kinetics fitting models, adsorption isotherm fitting models and thermodynamic parameters are listed in Additional file 1: SI. 4. Additionally, the models were analyzed using Origin 2021, and the average data and standard deviations were also reported. Error bars were used to represent standard deviations of multiple determinations.

3 Results and discussion

3.1 Characterization and formation of BC/rGA

As shown in the SEM images (Fig. 1), both rGA and BC/rGA had a 3D structure, which was similar to honeycomb briquette with well-developed pores. In addition, it could be clearly observed that there were interconnected pores on the surface of rGA, indicating that ions could continuously diffuse into the structure, which would greatly promote the adsorption process. But compared with rGA (Fig. 1a), the structural integrity of BC/rGA deteriorated and had partial collapse (Fig. 1b₁), so that the BC/rGA had larger surface area and smaller pores (Additional file 1: Fig. S5, Table S2). The average pore diameter of rGA and BC/rGA was 8.26 and 6.96 nm, respectively. Therefore, it could conclude that rGA and BC/rGA had mesoporous structures (Kaneko 1994). In addition, the surface of rGA was smooth, while the surface of BC/rGA was rough. Obviously, the presence of biochar can be observed in Fig. 1b₃ and c, which is similar to the results in the study of Wei et al. (2020), indicating the preparation of BC/rGA was successful.

FTIR spectra and XRD patterns are presented in Fig. 2. FTIR spectra (Fig. 2a) showed that BC, GO, rGA and BC/rGA had similar peaks, such as O–H stretching

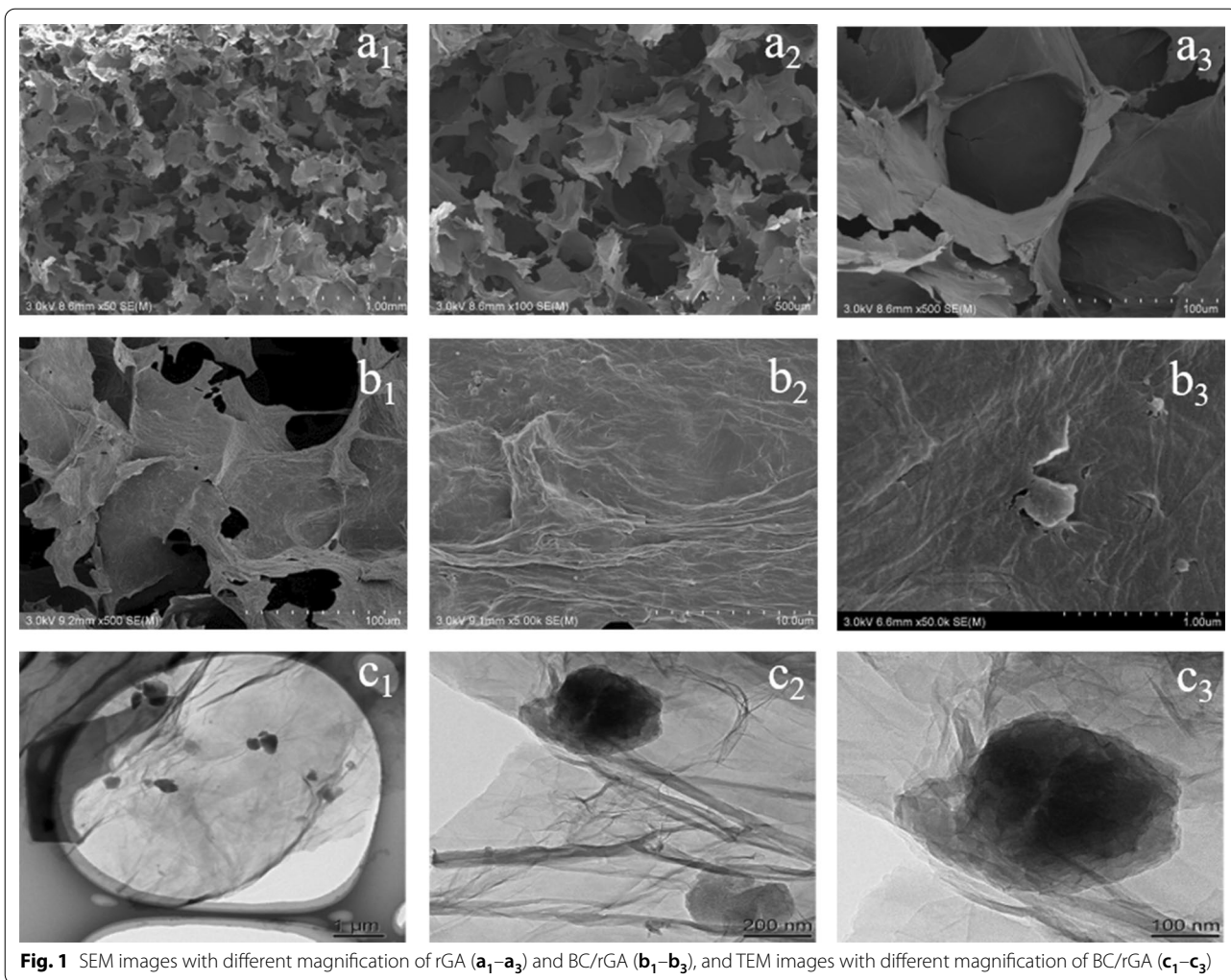


Fig. 1 SEM images with different magnification of rGA (a₁–a₃) and BC/rGA (b₁–b₃), and TEM images with different magnification of BC/rGA (c₁–c₃)

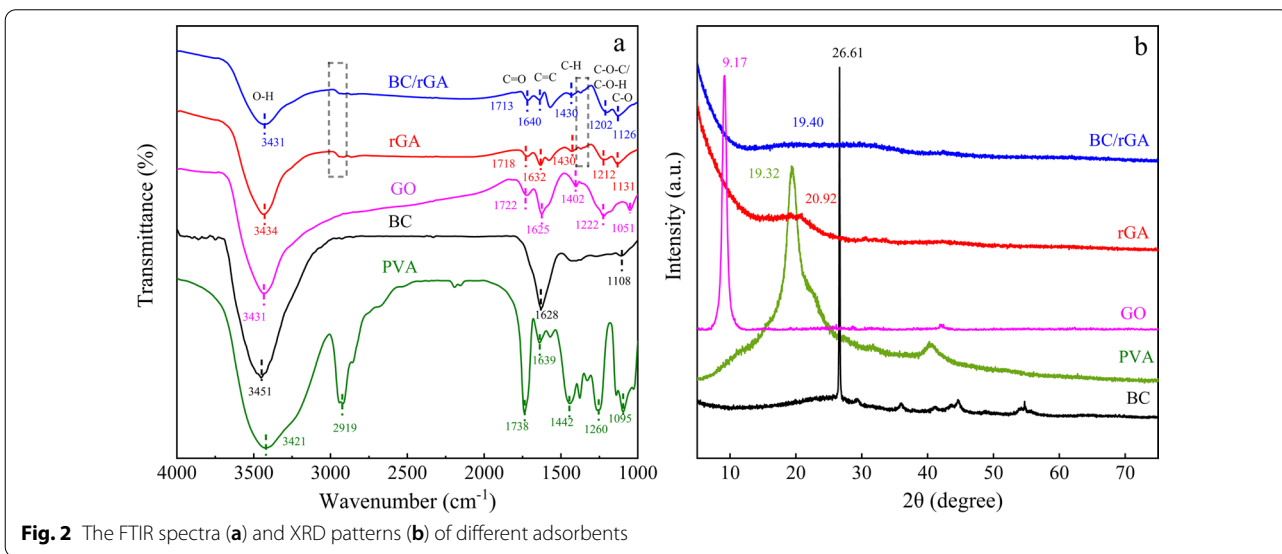


Fig. 2 The FTIR spectra (a) and XRD patterns (b) of different adsorbents

vibration bands around 3450 cm^{-1} . BC spectrum had three peaks at 3451 , 1628 and 1108 cm^{-1} , which represented O–H stretching vibration, aromatic C=C and –COOH (Ahmed et al. 2016; Fan et al. 2018). For the GO spectrum, the peaks at 3431 , 1722 , 1625 , 1402 , 1222 and 1051 cm^{-1} represented O–H stretching vibration, C=O stretching vibration from carboxylic groups, the carbon ring vibration of non-oxidized parts of GO (C=C), and the asymmetric bending of C–H, C–O–C or C–O–H group and C–O group (Peng et al. 2015; Wei et al. 2020; White et al. 2018), respectively. In addition, the PVA spectrum had peaks at around 3421 , 2919 , 1738 , 1639 , 1442 , 1260 and 1095 cm^{-1} . The FTIR spectra of aerogels were similar to GO and had some characteristic functional groups of GO, BC and PVA at the same time, while some functional groups were reduced and some peaks appeared. The intramolecular or intermolecular H bonds could enforce the inter-attraction between Cr(VI) and adsorbent which existed in the molecular foot (Wang et al. 2019). Compared with GO, the O–H stretching vibration peak intensity of aerogels decreased, and the bands between 1250 and 1050 cm^{-1} widened and shifted, indicating that the ether bonds were formed by the reaction between GO, PVA and aldehyde group in glutaraldehyde mixed solution (Ye et al. 2017; Hong et al. 2015). The peak intensity and wavenumber of C=O stretching vibration from carboxylic groups of GO, rGA and BC/rGA were changed. In addition, the bands at around 2900 and 1380 cm^{-1} (black rectangle in Fig. 2a) appeared because of the resonance between GO and PVA (Ye et al. 2017; Liu et al. 2021a, b). With the addition of biochar, the peak intensity of BC/rGA in O–H stretching vibration peak decreased, and the peak intensity decreased with the increase of biochar proportion (Additional file 1: Fig S6). However, the band intensity between 1000 and 1500 cm^{-1} was much larger than that of rGA, which indicated that ether bonds increased (Hong et al. 2015). This result might be due to the involvement of biochar in the acetal reaction.

The XRD patterns (Fig. 2b) showed that BC, GO and PVA had diffraction peak at 26.61° , 9.17° and 19.32° , respectively. The degree of peaks presented that GO had much larger interplanar spacing (0.96 nm) than that of pristine graphite (0.34 nm) (the calculations were shown in Additional file 1: SI. 5) because of the presence of oxygen groups on the surface of GO (Saleh et al. 2018; Zhang et al. 2015). However, the obvious typical diffraction peaks of GO and PVA disappeared in the XRD patterns of rGA and BC/rGA, indicating that the GO sheets were reduced and separated with the amorphous structure of PVA attached to the sheets (Bao et al. 2011). It could be found from the XRD pattern of rGA that there was a

wide peak at $2\theta = 20.92^\circ$ of rGA, implying that the layer spacing was 0.42 nm . The result also illustrated that the content of some oxygen groups decreased in the preparation process (Fadillah et al. 2019), which was consistent with the result of FTIR spectra. Compared with rGA, the characteristic peak ($2\theta = 19.40^\circ$) of BC/rGA shifted to the left and the layer spacing (0.46 nm) increased, which was attributed to the hydrogen bond between rGA and BC/rGA (Wei et al. 2020).

Raman spectra of aerogels (Additional file 1: Fig. S7) had D-band (around 1340 cm^{-1}) and G-band (around 1580 cm^{-1}). As it was well known, D-band represented the degree of disordered carbon or defect, which was mainly related to the vibration of carbon atoms with dangling bonds in the disordered carbon structure. G-band was almost attributed to the E_{2g} phonon mode of vibration of sp^2 C atoms in the 2D hexagonal lattice of a graphite cluster and could reflect the plane vibration of sp^2 carbon (Qu et al. 2013; Su et al. 2020; Sun et al. 2017). In this study, the value of I_D/I_G was 0.8483 and 0.8503 , respectively, indicating that there was no significant difference between the degree of graphitization of two tested adsorbents. The elemental composition of rGA and BC/rGA was analyzed by XPS, and the XPS spectra of C 1s and O 1s are shown in Additional file 1: Fig. S8. In the C 1s spectra, both rGA and BC/rGA had four peaks representing functional groups of C–C/C=C, C–O–C, C–O, C=O (Liao et al. 2018; Liu et al. 2021a, b; Singh et al. 2017), respectively. However, the proportion of C–O–C in BC/rGA was significantly higher than that of rGA, probably because BC also participated in the reaction to produce more ether groups. And the results were consistent with the results of FTIR.

The formation progress of BC/rGA is illustrated in the Fig. 3. After ball milling, biochar changed shape from plate to smaller granular, and increased SSA (from 14.02 to $351.58\text{ m}^2\text{ g}^{-1}$) and the amounts of surface functional groups (Additional file 1: Fig. S9), and it would take longer to sink in water (Additional file 1: Fig. S10). GO had a flake structure (Additional file 1: Fig. S11) and could be evenly dispersed in water for longer time than graphite (Additional file 1: Fig. S12). All these were conducive to manufacture BC/rGA. Under ultrasound and agitation, GO and BC were uniformly dispersed in the solution. The addition of glutaraldehyde mixed solution created acidic conditions. At this time, glutaraldehyde acted as an effective crosslinker to promote the effective connection of GO, PVA and BC through condensation reaction (Hong et al. 2015; Ye et al. 2017). GO sheets formed pores of various sizes, and the circled part in red in Fig. 3 presents the connection. The solution would fill the holes to

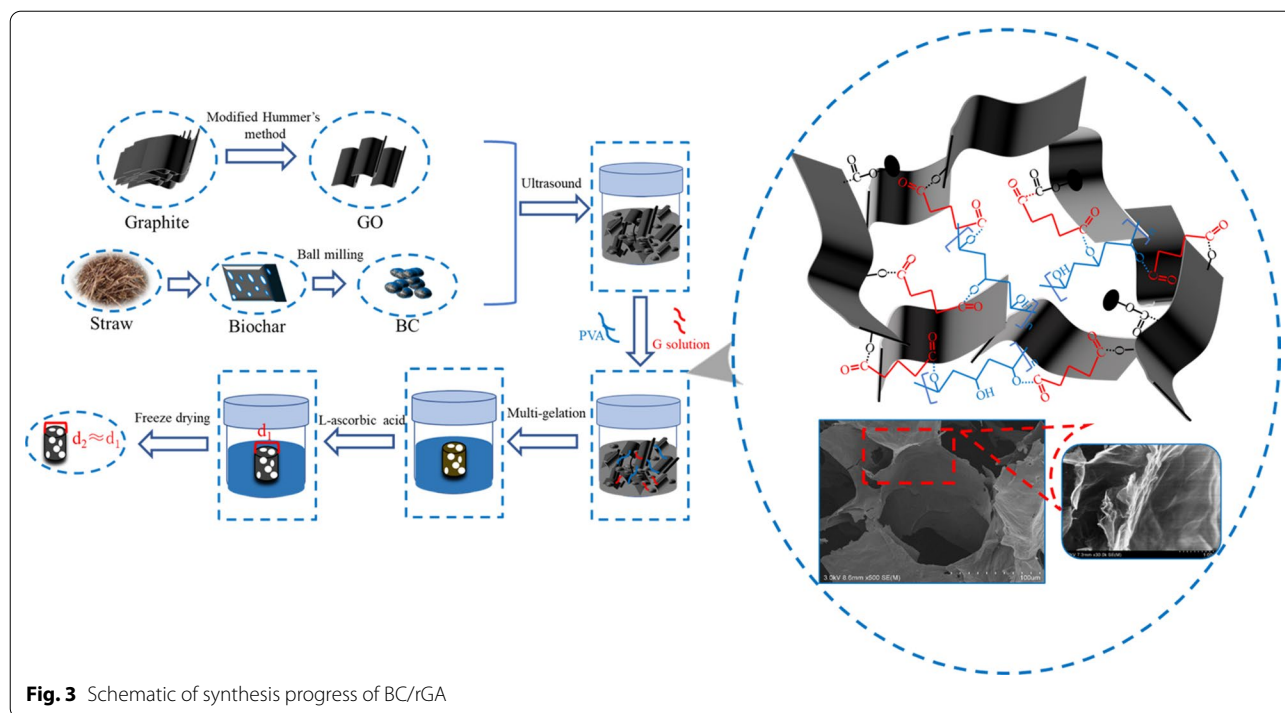


Fig. 3 Schematic of synthesis progress of BC/rGA

Table 1 Adsorption kinetic parameters of Cr(VI) on GO and aerogels

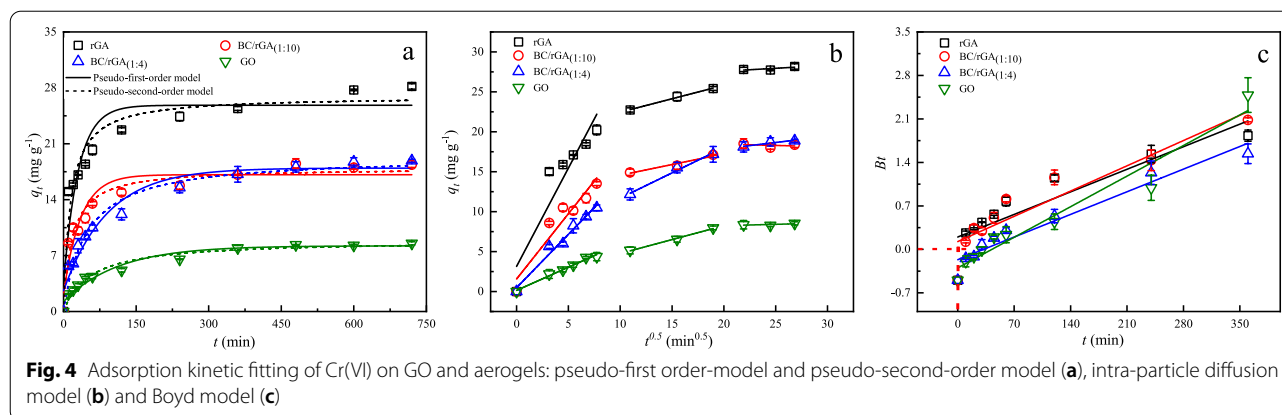
Adsorbents	Pseudo-first-order model			Pseudo-second-order model		
	Q_{e1} (mg g ⁻¹)	K_1 (min ⁻¹)	R^2_1	Q_{e2} (mg g ⁻¹)	K_2 (g mg ⁻¹ min ⁻¹)	R^2_2
GO	6.99	0.0089	0.955	8.90	2.04×10^{-3}	0.970
rGA	22.25	0.0327	0.890	26.95	2.61×10^{-3}	0.951
BC/rGA _(1:10)	14.91	0.0284	0.914	17.99	3.19×10^{-3}	0.962
BC/rGA _(1:4)	15.36	0.0110	0.956	19.43	1.10×10^{-3}	0.974

ensure that the connections between the GO would not break, and the pore structure of aerogel was basically formed. According to the previous study, the ice crystals could break through original network and eject graphene sheets into other ice crystals in the process of repeated freezing and thawing (Yang et al. 2015). Finally, the pores were connected to each other, which could promote the flow of solution, and the SEM images provided the direct evidence (Fig. 1). Due to the developed pore structure, the density of aerogels was small and the order of density was BC/rGA_(1:4) > BC/rGA_(1:2) > BC/rGA_(1:10) > rGA (Additional file 1: Fig. S13). The addition of L-ascorbic acid reduced GO to rGO, and made the structure more stable. Freeze-drying method could ensure the integrity of the structure, and resulted in no change in the diameter of the aerogel before (d_1) and after freeze-drying (d_2), indicating the aerogel did not shrink and deform any more (Chen et al. 2011; Shang et al. 2020; Ye et al. 2017).

3.2 Adsorption comparison

3.2.1 Adsorption kinetics of Cr(VI)

The adsorption equilibrium time of Cr(VI) on GO, rGA, BC/rGA_(1:10) and BC/rGA_(1:4) was about 8 h, and the equilibrium adsorption capacity (q_e) was 8.53, 28.18, 18.52 and 18.87 mg g⁻¹, respectively. The fitting results by pseudo-first-order and pseudo-second-order models (Table 1) showed that the adsorption rate and theoretical equilibrium adsorption capacity (Q_e) of aerogel were higher than those of GO. The 3D structure provided larger surface area and more adsorption sites for Cr(VI) adsorption (Hiew et al. 2018; Korkmaz and Kariper 2020; Zhang et al. 2018). Additionally, rGA showed the best adsorption performance, which might be because rGA had better structure than other adsorbents and more functional groups for adsorption. Compared with other graphene oxide composites (Neolaka et al. 2020, 2021), aerogels still had better adsorption capacity.



In addition, the pseudo-second-order model had higher correlation coefficient ($R^2 = 0.970, 0.951, 0.962, 0.974$), and the calculated adsorption capacity ($8.90, 26.95, 17.99$ and 19.43 mg g^{-1}) was closer to the experimental value ($8.53, 28.18, 18.52$ and 18.87 mg g^{-1}) for GO, rGA, BC/rGA_(1:10) and BC/rGA_(1:4), which indicated that chemisorption also took part in this adsorption process (Chen et al. 2011). Based on the model assumptions, chemical adsorption might limit the rate involving valence forces through sharing or exchange of electrons between Cr(VI) and adsorbents (GO, rGA and BC/rGA) (Liang et al. 2018; Li et al. 2020; Mo et al. 2019; Pang et al. 2011).

In order to further clarify the Cr(VI) adsorption process and adsorption kinetics, the inter-particle diffusion model and Boyd model were adopted. Figure 4 shows the intra-particle diffusion of GO, rGA and BC/rGA, which was divided into three parts. The fitting parameters are listed in Additional file 1: Table S3 and showed that the intercepts of each part were not zero, indicating that intraparticle diffusion was not the only rate control step in the adsorption process (Li et al. 2020). The first section represented the movement of Cr(VI) ions from the solution to the surface of the adsorbents and was referred to liquid film diffusion. This section had the largest slope, which was due to the large concentration gradient at the beginning (Behnajady and Bimeghdar 2014; Wang et al. 2021). In the second stage of the model, Cr(VI) ions moved towards the adsorption sites and were adsorbed. This process was corresponded to an intra particle diffusion process, which was obviously slower than liquid film diffusion, indicating that the adsorption rate was mainly controlled by internal diffusion process (Hu et al. 2011). And then, the adsorption finally reached the equilibrium. In addition, the Boyd model results are shown in Fig. 4. The results showed that B_t and t had a good linear relationship, but the line did not pass through the origin, which further proved that liquid film diffusion was also one of the rate command steps in the adsorption progress (Li et al. 2020).

In summary, the adsorption process of Cr(VI) on aerogel was a multi-step process, and the adsorption rate was affected by a variety of mechanisms, mainly depending on the pore diffusion and chemisorption process. Compared with other adsorbents (Additional file 1: Table S4), rGA and BC/rGA had better adsorption capacity and could be directly separated from solution using tweezer, not by filtration or centrifugation.

3.2.2 Adsorption isotherms of Cr(VI)

The adsorption capacity of different adsorbents for Cr(VI) at different concentrations following the order of $\text{rGA} > \text{BC/rGA}_{(1:4)} > \text{BC/rGA}_{(1:10)} > \text{GO}$. When the initial concentration of Cr(VI) solution was 100 mg L^{-1} , the adsorption capacity of rGA, BC/rGA_(1:4) and BC/rGA_(1:10) was 3.38, 1.29, and 2.23 times higher than that of GO, respectively. In the setting concentration range, the adsorption of Cr(VI) on the four adsorbents increased with the increasing concentration. This was because under the high concentration, Cr(VI) ions were more likely to collide with the adsorbent, and the adsorption capacity increased accordingly (Hasanpour and Hatami 2020). The adsorption capacity of rGA, BC/rGA_(1:4), BC/rGA_(1:10) and GO increased 3.81, 2.96, 6.08 and 1.55 times with the initial concentration of Cr(VI) increasing from 10 mg L^{-1} to 100 mg L^{-1} . However, due to the limited adsorption sites, the increase intensity of adsorption capacity gradually decreased, especially the GO. When the initial concentration of Cr(VI) solution was 10 mg L^{-1} , the q_e of rGA, BC/rGA_(1:4) and GO was $6.75, 3.41$ and 2.93 mg g^{-1} , respectively. The cycle adsorption experiment was carried out on the adsorbent (Additional file 1: Fig. S14). In the fifth cycle of adsorption, the adsorption capacity of Cr(VI) by rGA decreased by 45% and that of BC/rGA_(1:4) decreased by 39%. In each of the three previous adsorption processes, the difference between rGA and BC/rGA_(1:4) adsorption capacity was similar. When the recycling of adsorbents was

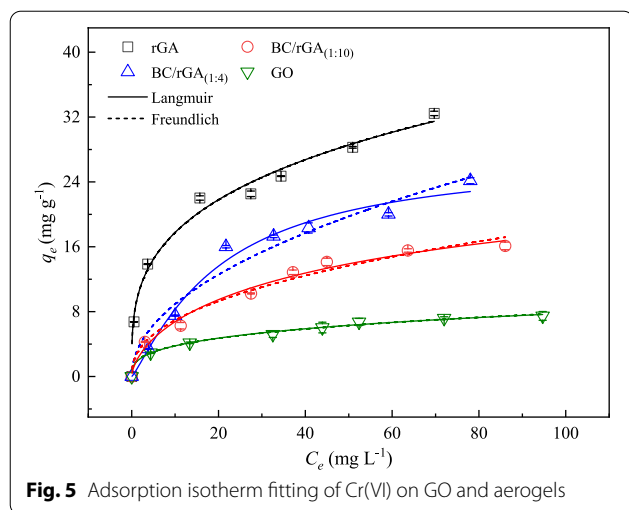


Fig. 5 Adsorption isotherm fitting of Cr(VI) on GO and aerogels

not considered, 0.75 g rGA (0.283 g GO) and 1.47 g BC/rGA_(1:4) (0.276 g GO and 0.069 g BC) and 1.71 g GO were required to treat a litre Cr(VI) solution from 10 mg L⁻¹ to 5 mg L⁻¹ (the first adsorption capacity was taken as the parameter). Notably, the density of rGA and BC/rGA and the weight of PVA should also be considered in the calculation of the results. The difference of adsorption capacity between rGA and BC/rGA_(1:4) became smaller, and the fifth adsorption capacity of the two adsorbents in fifth cycle was close to each other, which could better illustrate the economy of BC/rGA_(1:4). Therefore, BC/rGA_(1:4) could not only save the cost of solid–liquid separation, but also reduce the use of GO to reduce the adsorbent cost.

Adsorption isotherm models were used to further understand the adsorption behaviors and mechanisms involved in interaction between Cr(VI) and adsorbents. Isothermal adsorption fitting curves of GO, rGA and BC/rGA at room temperature are shown in Fig. 5, and relevant parameters of fitting results are listed in Table 2. The results showed that the constant N values of the Freundlich model for the four adsorbents were in the range of 2–10, indicating that the adsorption reaction was easy (Wang et al. 2014, 2021; Xu et al. 2015). In addition, Langmuir model ($R^2 > 0.974$) fitted the data better than

Freundlich model ($R^2 > 0.946$), implying that the adsorption of Cr(VI) on the adsorbent was dominated by monolayer adsorption (Wang et al. 2021) and homogeneous adsorption (Guo et al. 2018).

Comparing the adsorption kinetics and isothermal adsorption of the four adsorbents, aerogels had faster adsorption rate and larger adsorption capacity than GO, which indicated that the 3D structure of aerogel could ensure excellent adsorption performance. And BC/rGA_(1:4) had higher adsorption capacity than BC/rGA_(1:10), where the ratio of BC to GO was 1:4 as the preparation scheme of BC/rGA. In addition, the model fitting results showed that the adsorption progresses of Cr(VI) on those four adsorbents were dominated by monolayer adsorption involving chemisorption, and the adsorption rate was controlled by the pore diffusion and chemisorption process.

3.3 Effect of environmental factors on Cr(VI) adsorption

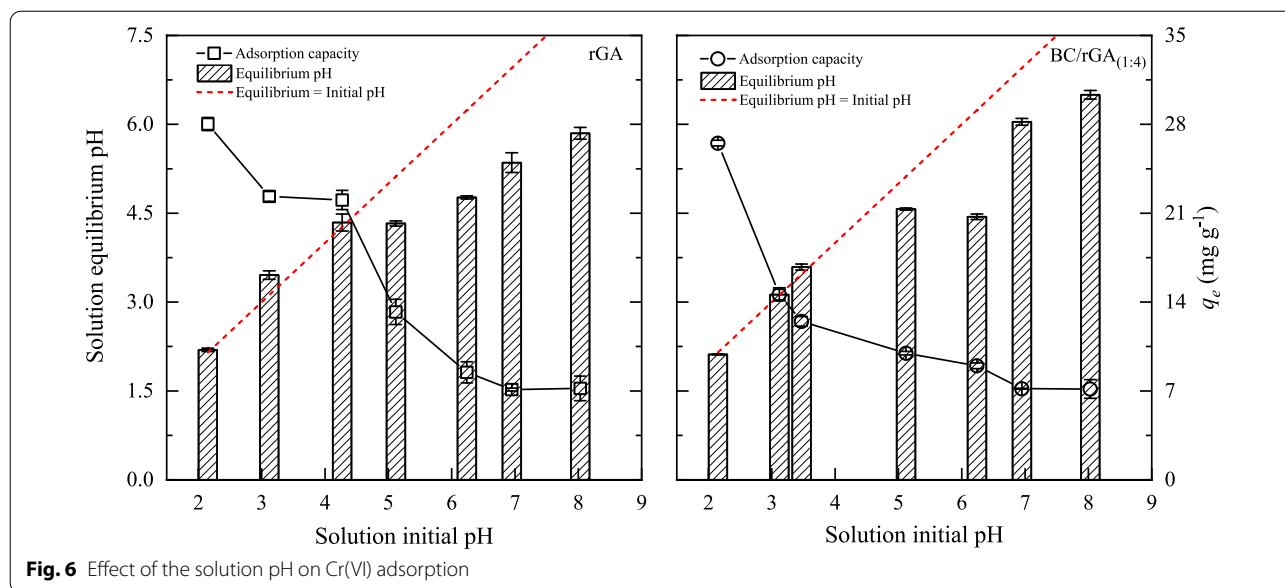
3.3.1 Effect of solution pH on Cr(VI) adsorption

Obviously, solution pH had a great effect on Cr(VI) adsorption within the range of pH 2–8, and the adsorption capacity was negatively correlated with solution pH value (Fig. 6). The adsorption capacity reached the maximum at pH 2, and the adsorption capacity at pH 8 was only 25.68% and 26.98% of that at pH 2 for rGA and BC/rGA_(1:4), respectively. The results indicated that the solution pH value played a vital role on the adsorption capacity of Cr(VI), which was consistent with the previous studies (Rajapaksha et al. 2018; Su et al. 2020; Zhou et al. 2016).

The effect of solution pH value on adsorption mainly included the alteration of the adsorbent surface properties and valence states of heavy metals (Guo et al. 2018; Wang et al. 2021). The different properties of the adsorbent surface could consequently affect the electrostatic interaction between the adsorbent and heavy metals (Mukherjee et al. 2011; Wang et al. 2021). According to previous studies (Liang et al. 2018; Wang et al. 2014), the main forms of Cr(VI) were HCrO_4^- and $\text{Cr}_2\text{O}_7^{2-}$ and the surfaces of rGA and BC/rGA_(1:4) were positively charged at pH 2 (Additional file 1: Fig. S15). The adsorbate could be adsorbed by electrostatic attraction. In addition, the

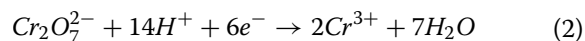
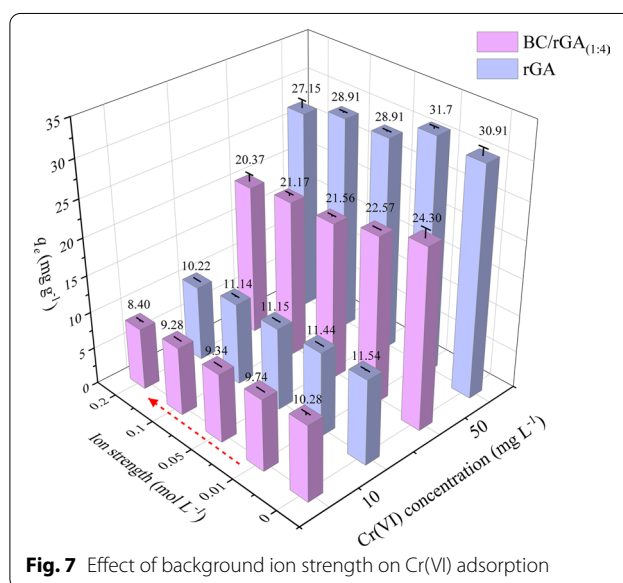
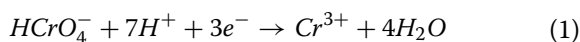
Table 2 Adsorption isotherm parameters of Cr(VI) adsorption on GO and aerogels

Adsorbents	Freundlich			Langmuir		
	N	K_F ($\text{mg}^{(1-1/n)} \text{L}^{1/n} \text{g}^{-1}$)	R^2	Q_m (mg g^{-1})	K_L (L mg^{-1})	R^2
GO	3.18	1.84	0.984	45.38	0.04	0.984
rGA	2.50	6.64	0.970	51.40	0.04	0.999
BC-rGA _(1:10)	2.38	2.64	0.966	32.71	0.06	0.974
BC-rGA _(1:4)	2.44	5.36	0.946	39.97	0.02	0.988



high concentration of H⁺ in the vicinity of adsorbents could increase the electrostatic attraction between H⁺ and HCrO₄⁻ to promote the adsorption process (Dubey et al. 2015). And the protonation of surface functional groups could effectively adsorb Cr(VI) at pH 2 (Xu et al. 2015; Yang et al. 2018). Therefore, the adsorption capacity remained a high level at pH 2. The surfaces of rGA and BC/rGA_(1:4) were electronegative when pH value was greater than 2, and the electronegativity increased with the increasing solution pH value. Moreover, the decrease of adsorption capacity might be related to the reduced degree of the protonation or the deprotonation of rGA and BC/rGA_(1:4) (Dong et al. 2016; Guo et al. 2018; Lu et al. 2017). Then, the electrostatic repulsion between adsorbents and Cr(VI) anions increased, and the adsorption capacity eventually decreased.

It could be seen from Fig. 6 that the solution pH value changed before and after adsorption. In the solution with low PH value (pH < 4), equilibrium pH value was greater than the initial pH value. This was because that H⁺ was consumed in the solution, partly for Cr(VI) reduction (Eqs. 1, 2) and partly for protonation of surface functional groups (Guo et al. 2018; Singh et al. 2017; Xu et al. 2015). In the solution with high PH value (pH > 4), equilibrium pH value was less than the initial pH value. Cr(III) ions could convert to Cr(OH)₃ by combining with OH⁻ (Chen et al. 2015), and the functional groups on the adsorbent surface could hydrolyze to produce H⁺, which resulted in a decrease in the pH value of solution.



3.3.2 Effect of background ion strength on Cr(VI) adsorption
 The adsorption capacity of Cr(VI) on rGA and BA/rGA_(1:4) could also be affected by the background ion strength, and the effect trends were similar (Fig. 7). In this work, the adsorption process of Cr(VI) was almost unaffected at a concentration of 10 mg L⁻¹, while the adsorption capacity of Cr(VI) on rGA and BA/rGA_(1:4) decreased with the increasing ionic strength at a high Cr(VI) concentration (50 mg L⁻¹). When the background

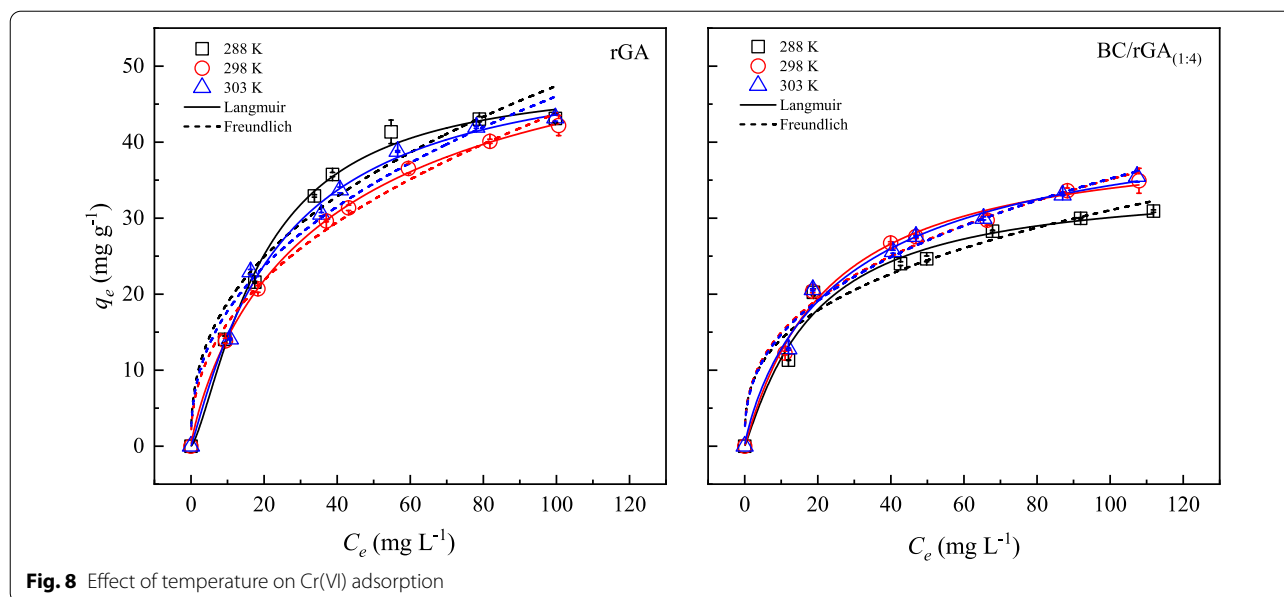


Fig. 8 Effect of temperature on Cr(VI) adsorption

ion strength increased from 0.001 mol L^{-1} to 0.2 mol L^{-1} , the Cr(VI) removal amount decreased by 12.16% (rGA) and 16.19% (BC/rGA_(1:4)).

The effect of ionic strength on the adsorption of Cr(VI) using rGA and BA/rGA_(1:4) was investigated at pH 2. There were two competitive relationships in the solution, the competition between Na^+ and Cr(III), and the competition between Cl^- and HCrO_4^- or $\text{Cr}_2\text{O}_7^{2-}$. When the concentration of Cr(VI) was low, the adsorption sites were relatively enough, and the adsorption processes of rGA and BA/rGA_(1:4) were slightly affected. In the high Cr(VI) concentration solution, the increasing background ion strength enhanced the competition, and the adsorption capacity decreased accordingly.

3.3.3 Effect of temperature on Cr(VI) adsorption and adsorption thermodynamics

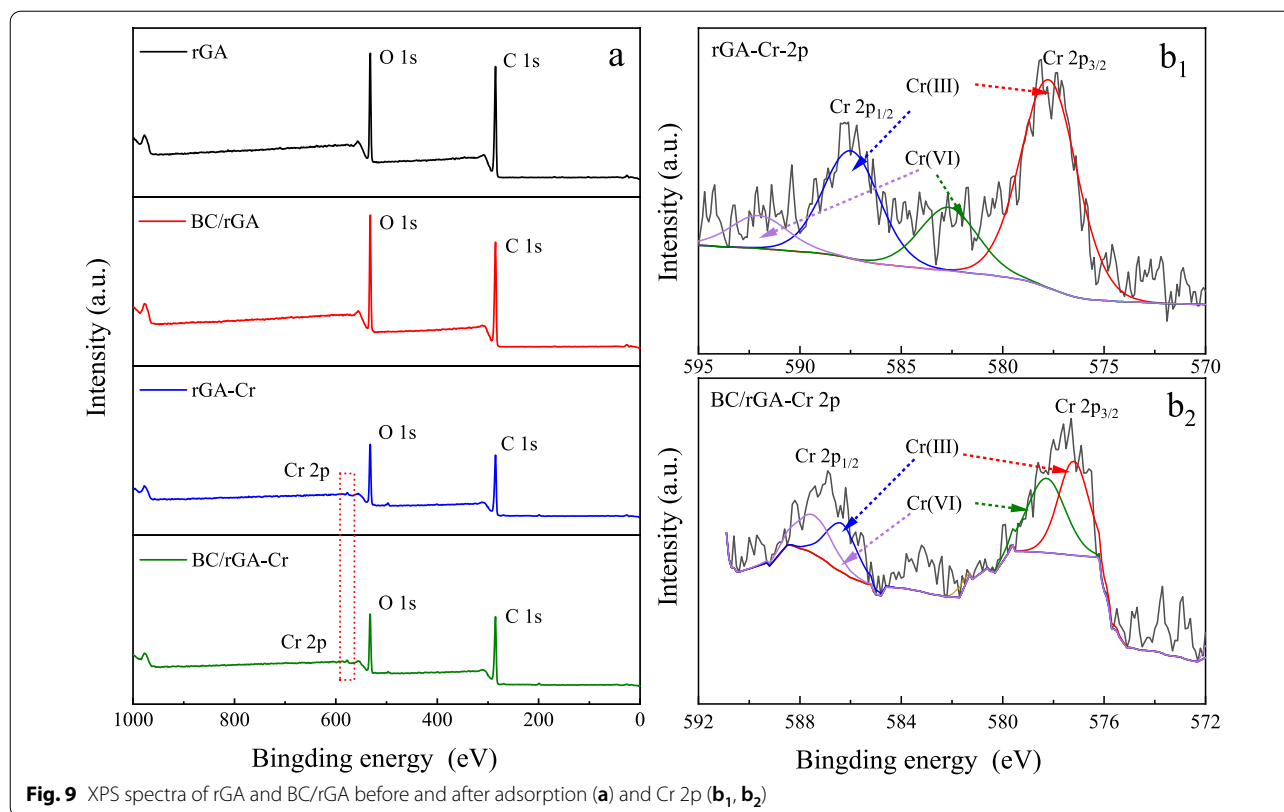
In this work, the equilibrium adsorption capacity of rGA and BC/rGA_(1:4) slightly increased with the increasing temperature, which might be due to the increased diffusion of Cr(VI) ions in the solution (Mukherjee et al. 2011). Figure 8 shows the isothermal adsorption plots of rGA and BC/rGA_(1:4) at three temperatures (288 K, 298 K, 303 K), and the relevant fitting parameters are presented in Additional file 1: Table S5. For rGA and BC/rGA_(1:4), the R^2 of Langmuir model was higher than that of Freundlich model at three temperatures, which was consistent with the previous isothermal results (Table 2).

In order to further explain the variation of adsorption capacity, thermodynamic parameters were also calculated. And the related equations and parameters are given in Additional file 1: SI.7. The results showed

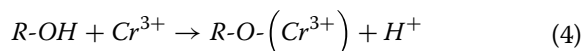
that ΔG became more negative with rising temperature, indicating that the adsorption process was spontaneous (Saleh et al. 2018; Singh et al. 2017; Wang et al. 2014) and the degree of spontaneity increased with the increase of temperature (Huang et al. 2018). The positive value ΔH reflected that the adsorption was endothermic reaction, which was consistent with the research results in literature (Liang et al. 2018; White et al. 2018). The ΔS was also positive value, indicating that the disorder degree of solid/liquid interface increased during the adsorption of Cr(VI) (Hu et al. 2011; Liang et al. 2018; Singh et al. 2017).

3.4 Adsorption mechanism

In the XPS spectra of rGA and BC/rGA before and after adsorption (Fig. 9a), Cr 2p appeared after the adsorption, indicating that the aerogel successfully adsorbed chromium. And two characteristic peaks of Cr 2p_{3/2} and Cr 2p_{1/2} could be observed in the Cr 2p spectra (Fig. 9b). In the Cr 2p spectrum of rGA (rGA-Cr), the two characteristic peaks could be divided into four peaks, which represented Cr(III) at 577.72 and 587.46 eV, and Cr(VI) at 582.66 and 592.01 eV (Luo et al. 2021; Wang et al. 2021; Wei et al. 2020). The Cr 2p spectrum of BC/rGA (BC/rGA-Cr) was similar that of rGA-Cr, and had Cr(III) peaks (at 577.20 and 586.36 eV) and Cr(VI) peaks (at 577.20 and 586.36 eV). The results showed that Cr(III) existed on the adsorbents after the adsorption, and there were two main reasons for the appearance of Cr(III). On the one hand, Cr(VI) had higher redox(oxidation/reduction) potential value under standard conditions, and Cr(VI) could be reduced to Cr(III) (Tran et al. 2017; Vo



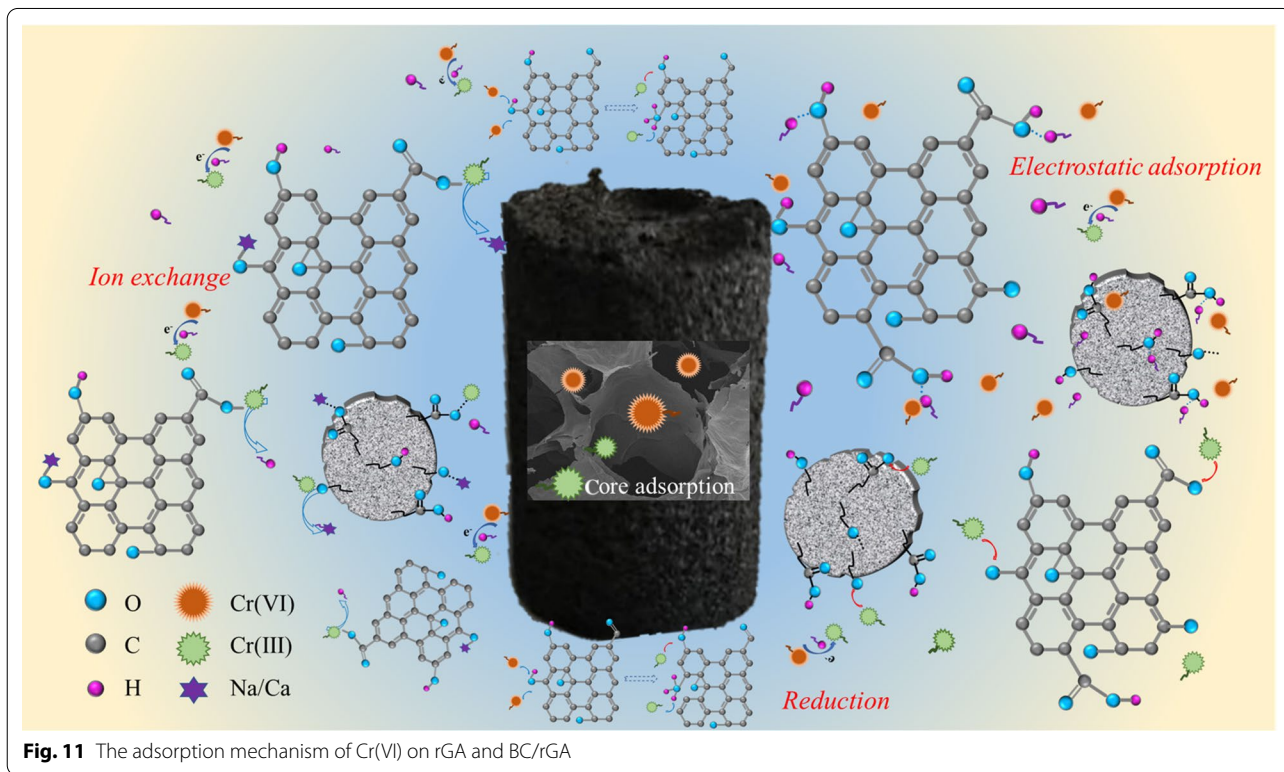
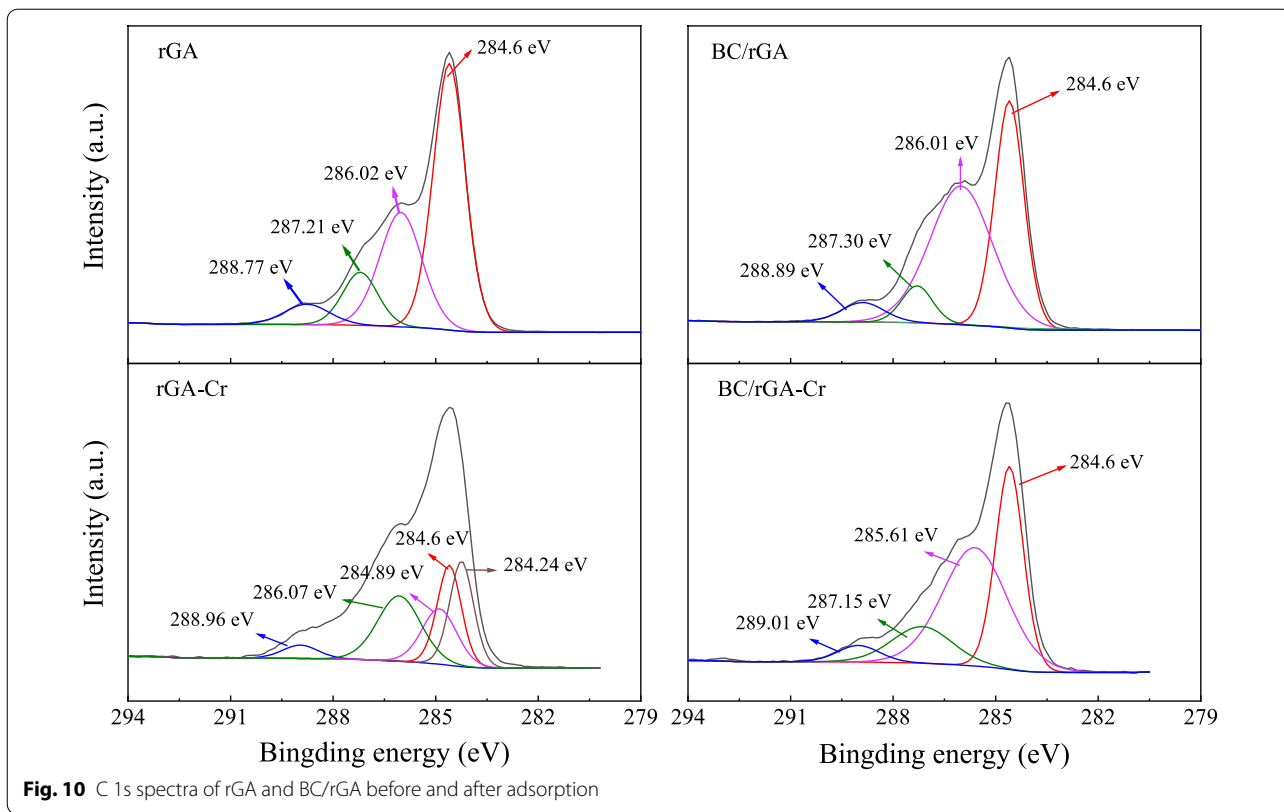
et al. 2019). The carbon–carbon bond of the graphene ring was broken, and the adsorbed Cr(VI) was reduced to Cr(III) by the π electrons (Wang et al. 2017b; Wei et al. 2020), and then Cr(III) was adsorbed. On the other hand, Cr(III) obtained by the reduction of Cr(VI) in low pH value environment (Eqs. 1, 2) was directly adsorbed on rGA and BA/rGA (Li et al. 2017; Liang et al. 2018; Wei et al. 2020). Cr(III) was one of the less toxic species, so the reduction could be regarded as a major strategy to reduce the adverse environmental effects of chromium (Li et al. 2021; Qiu et al. 2022; Su et al. 2021). With the solution pH value increasing, Cr(III) could be adsorbed by electrostatic action on the adsorbent surface (Fig. 7). In addition, Cr(III) could also be adsorbed by ion exchange (Eqs. 3, 4) or coordination reactions (Guo et al. 2018; Huang et al. 2018; Mei et al. 2020) by functional groups in the adsorbent surface.



The positions and contents of different functional groups had changed in the spectra of C 1s and O 1s of

rGA and BC/rGA after the adsorption (Fig. 10, Additional file 1: Figs. S8, S16). The C=O binding energies of rGA and BC/rGA were 288.77 eV and 288.89 eV before adsorption and increased to 288.96 eV and 289.01 eV after the adsorption, respectively. This indicated that functional groups were involved in chemical reactions during the adsorption and acted electron donors for the reduction of Cr(VI) to be Cr(III) (Yang et al. 2018). The binding energy of O 1s moved to the higher binding energy direction, which was similar to the study of Cr(VI) removal by chitosan aerogel (Wang et al. 2021), which implied that the O element might be involved in the oxidation mechanism caused by Cr(VI) (Huang et al. 2018; Mei et al. 2020). Moreover, the reduction of Cr(VI) to Cr(III) is also suggested by Fig. 10 and Additional file 1: Fig. S8. With the oxidation of C–C, the ratio of C–O, C=O and O–C=O peaks inversely increased. In addition, the surfaces of rGA and BC/rGA were positively charged at low pH value (Additional file 1: Fig. S15) and surface functional groups could also be protonated ($-COOH_2^+$, $-OH_2^+$) (Liao et al. 2018; Xu et al. 2015; Yang et al. 2018) to adsorb Cr(VI) by electrostatic interaction.

In summary, the adsorption mechanisms of Cr(VI) on rGA and BC/rGA mainly included three reactions in this work (Fig. 11). The reduction reaction of Cr(VI) to Cr(III), the electrostatic adsorption between Cr(VI), Cr(III) and



surface functional groups, and the ion exchange between Cr(III) and cations on functional groups. The results were consistent with the confirmed conclusion in previous studies (Liang et al. 2021; Lu et al. 2022; Su et al. 2020) that the interaction between adsorbents and inorganic pollutants was generally attributed to ion exchange, surface complexation, (co)precipitation, etc.

4 Conclusion and prospect

In this study, BC/rGA with a stable 3D structure and well-developed pores was successfully prepared with the freeze-thawing technique and sol-gel method by mixing BC and GO in a certain proportion and using PVA as an effective binder, which could be directly removed from the solution to achieve solid-liquid separation. BC/rGA had a similar structure and some characteristic functional groups of GO, BC and PVA at the same time, which made the adsorption capacity of binary composites aerogel three times that of GO.

Although the adsorption was affected by solution pH, electrolyte ion strength and temperature, BC/rGA was regarded as a green and economical adsorbent, especially when the blending ratio of BC and GO was 1:4. Generally, ball-milled biochar was a great option of additive material for the graphene-based composite aerogel preparation, and BC/rGA could be used as a promising green adsorbent for water treatment, not only used to remove heavy metals from solution. At the same time, the application of BC/rGA could not only save the cost of solid-liquid separation and reduce the use of GO, but also promote the effective utilization of agricultural waste and reduce the environmental pressure. Future research should focus on BC/rGA modification to promote performance optimization, the application in other contaminant removal and the preparation of aerogel with lower cost and better performance, which will be beneficial to efficiently achieve contaminated water treatment.

Supplementary Information

The online version contains supplementary material available at <https://doi.org/10.1007/s42773-022-00191-w>.

Additional file 1. The additional file contains the preparation of adsorbents, the data analysis, the characterization of adsorbents, the cycle adsorption capacity of adsorbents, and the kinetic, isotherm and thermodynamic parameters for chromium adsorption. The additional file includes six tables and sixteen figures.

Acknowledgements

This work was supported by the National Natural Science Foundation of China (Grant No. 21377074). Additionally, we are all extremely grateful to the editor and anonymous reviewers for their helpful comments.

Author contributions

NC(Naiju Che): conceptualization, sampling, analysis, investigation, visualization, writing original draft and review. NL(Na Liu): analysis, investigation and review and editing. YL (Yinhui Li): sampling, analysis and investigation. CL (Chao Li): sampling and investigation. YL (Yanli Liu): analysis, review and editing and supervision. CL (Chengliang Li): review and editing, supervision, project administration and funding acquisition. All authors read and approved the final manuscript.

Funding

This work was funded by the National Natural Science Foundation of China (Grant No. 21377074).

Availability of data and materials

All data generated or used during the study appear in the submitted article.

Declarations

Competing interests

The authors declare that they have no competing interests.

Received: 28 July 2022 Revised: 5 November 2022 Accepted: 14 November 2022

Published online: 08 December 2022

References

- Ahmed MB, Zhou JL, Ngo HH, Guo WS, Chen MS (2016) Progress in the preparation and application of modified biochar for improved contaminant removal from water and wastewater. *Bioresour Technol* 214:836–851. <https://doi.org/10.1016/j.biortech.2016.05.057>
- Bao CL, Guo YQ, Song L, Hu Y (2011) Poly (vinyl alcohol) nanocomposites based on graphene and graphite oxide: a comparative investigation of property and mechanism. *J Mater Chem* 21(36):13942–13950. <https://doi.org/10.1039/c1jm11662b>
- Behnajady MA, Bimeghdar S (2014) Synthesis of mesoporous NiO nanoparticles and their application in the adsorption of Cr(VI). *Chem Eng J* 239:105–113. <https://doi.org/10.1016/j.cej.2013.10.102>
- Chen N, Zhang ZY, Feng CP, Zhu DR, Yang YN, Sugiura N (2011) Preparation and characterization of porous granular ceramic containing dispersed aluminum and iron oxides as adsorbents for fluoride removal from aqueous solution. *J Hazard Mater* 186(1):863–868. <https://doi.org/10.1016/j.jhazmat.2010.11.083>
- Chen T, Zhou ZY, Xu S, Wang HT, Lu WJ (2015) Adsorption behavior comparison of trivalent and hexavalent chromium on biochar derived from municipal sludge. *Bioresour Technol* 190:388–394. <https://doi.org/10.1016/j.biortech.2015.04.115>
- Chen HB, Gao YR, Li JH, Sun CH, Sarkar B, Bhatnagar A, Bolan N, Yang X, Meng J, Liu ZZ, Hou H, Wong JWC, Hou DY, Chen WF, Wang HL (2022) Insights into simultaneous adsorption and oxidation of antimonite [Sb(III)] by crawfish shell-derived biochar: spectroscopic investigation and theoretical calculations. *Biochar* 4:37. <https://doi.org/10.1007/s42773-022-00161-2>
- Dai WJ, Xu ML, Zhao ZL, Zheng JT, Huang F, Wang H, Liu CF, Xiao RB (2021) Characteristics and quantification of mechanisms of Cd²⁺ adsorption by biochars derived from three different plant-based biomass. *Arab J Chem* 14:103119. <https://doi.org/10.1016/j.arabjch.2021.103119>
- Dong Z, Zhao J, Du JF, Li CC, Zhao L (2016) Radiation synthesis of spherical cellulose-based adsorbent for efficient adsorption and detoxification of Cr(VI). *Radiat Phys Chem* 126:68–74. <https://doi.org/10.1016/j.radphyschem.2016.05.013>
- Dubey R, Bajpai J, Bajpai AK (2015) Green synthesis of graphene sand composite (GSC) as novel adsorbent for efficient removal of Cr(VI) ions from aqueous solution. *J Water Process Eng* 5:83–94. <https://doi.org/10.1016/j.jwpe.2015.01.004>
- Fadillah G, Saleh TA, Wahyuningsih S, Putric ENK, Febrianastuti S (2019) Electrochemical removal of methylene blue using alginate-modified graphene

- adsorbents. *Chem Eng J* 378:122140. <https://doi.org/10.1016/j.cej.2019.122140>
- Fan ZX, Zhang Q, Gao B, Li M, Liu CY, Qiu Y (2018) Removal of hexavalent chromium by biochar supported nZVI composite: batch and fixed-bed column evaluations, mechanisms, and secondary contamination prevention. *Chemosphere* 217:85–94. <https://doi.org/10.1016/j.chemosphere.2018.11.009>
- Guo DM, An QD, Xiao ZY, Zhai SR, Yang DJ (2018) Efficient removal of Pb(II), Cr(VI) and organic dyes by polydopamine modified chitosan aerogels. *Carbohydr Polym* 202:306–314. <https://doi.org/10.1016/j.carbpol.2018.08.140>
- Gupta S, Sireesha S, Sreedhar I, Patel CM, Anitha KL (2020) Latest trends in heavy metal removal from wastewater by biochar based sorbents. *J Water Process Eng* 38:101561. <https://doi.org/10.1016/j.jwpe.2020.101561>
- Hasanpour M, Hatami M (2020) Application of three dimensional porous aerogels as adsorbent for removal of heavy metal ions from water/wastewater: a review study. *Adv Colloid Interface Sci* 284:102247. <https://doi.org/10.1016/j.cis.2020.102247>
- Hiew BYZ, Lee LY, Lee XJ, Thangalazhy-Gopakumar S, Gan SY, Lim SS, Pan GT, Yang CK, Chiu WS, Khiew PS (2018) Review on synthesis of 3D graphene-based configurations and their adsorption performance for hazardous water pollutants. *Process Saf Environ* 116:262–286. <https://doi.org/10.1016/j.psep.2018.02.010>
- Hong JY, Bak BM, Wie JJ, Kong J, Park HS (2015) Reversibly compressible, highly elastic, and durable graphene aerogels for energy storage devices under limiting conditions. *Adv Funct Mater* 25(7):1053–1062. <https://doi.org/10.1002/adfm.201403273>
- Hu XJ, Wang JS, Liu YG, Li X, Zeng GM, Bao ZL, Zeng XX, Chen AW, Long F (2011) Adsorption of chromium(VI) by ethylenediamine-modified cross-linked magnetic chitosan resin: isotherms, kinetics and thermodynamics. *J Hazard Mater* 185:306–314. <https://doi.org/10.1016/j.jhazmat.2010.09.034>
- Hu BW, Ai YJ, Jin J, Hayat T, Alsaedi A, Zhuang L, Wang XK (2020) Efficient elimination of organic and inorganic pollutants by biochar and biochar-based materials. *Biochar* 2:47–64. <https://doi.org/10.1007/s42773-020-00044-4>
- Huang YM, Lee XQ, Macazo FC, Grattieri M, Cai R, Minter SD (2018) Fast and efficient removal of chromium(VI) anionic species by a reusable chitosan-modified multi-walled carbon nanotube composite. *Chem Eng J* 339:259–267. <https://doi.org/10.1016/j.cej.2018.01.133>
- Joseph L, Jun BM, Flora JRV, Park CM, Yoon Y (2019) Removal of heavy metals from water sources in the developing world using low-cost materials: a review. *Chemosphere* 229:142–159. <https://doi.org/10.1016/j.chemosphere.2019.04.198>
- Kaneko K (1994) Determination of pore size and pore size distribution: 1. Adsorbents and catalysts. *J Membr Sci* 96(1–2):59–89. [https://doi.org/10.1016/0376-7388\(94\)00126-X](https://doi.org/10.1016/0376-7388(94)00126-X)
- Kořowski M, Hilber I, Bucheli TD, Charmas B, Skubiszewska-Zięba J, Oleszczuk P (2017) Activated biochars reduce the exposure of polycyclic aromatic hydrocarbons in industrially contaminated soils. *Chem Eng J* 310:33–40. <https://doi.org/10.1016/j.cej.2016.10.065>
- Korkmaz S, Kariper A (2020) Graphene and graphene oxide based aerogels: synthesis, characteristics and supercapacitor applications. *J Energy Storage* 27:101038. <https://doi.org/10.1016/j.est.2019.101038>
- Lee JH, Park SJ (2020) Recent advances in preparations and applications of carbon aerogels: a review. *Carbon* 163:1–18. <https://doi.org/10.1016/j.carbon.2020.02.073>
- Leng LJ, Xiong Q, Yang LH, Li H, Zhou YY, Zhang WJ, Jiang SJ, Li HL, Huang HJ (2021) An overview on engineering the surface area and porosity of biochar. *Sci Total Environ* 763:144204. <https://doi.org/10.1016/j.scitotenv.2020.144204>
- Li X, Wang J (2020) One-dimensional and two-dimensional synergized nanostructures for high-performing energy storage and conversion. *InfoMat* 2:3–32. <https://doi.org/10.1002/inf2.12040>
- Li LL, Feng XQ, Han RP, Zang SQ, Yang G (2017) Cr(VI) removal via anion exchange on a silver-triazolate MOF. *J Hazard Mater* 321:622–628. <https://doi.org/10.1016/j.jhazmat.2016.09.029>
- Li CJ, Zhang L, Gao Y, Li AM (2018) Facile synthesis of nano ZnO/ZnS modified biochar by directly pyrolyzing of zinc contaminated corn stover for Pb(II), Cu(II) and Cr(VI) removals. *Waste Manag* 79:625–637. <https://doi.org/10.1016/j.wasman.2018.08.035>
- Li LY, Cao G, Zhu RS (2020) Adsorption of Cr(VI) from aqueous solution by a litchi shell-based adsorbent. *Environ Res* 196:110356. <https://doi.org/10.1016/j.envres.2020.110356>
- Li Y, Xiong W, Wei X, Qin J, Lin C (2021) Transformation and immobilization of hexavalent chromium in the co-presence of biochar and organic acids: effects of biochar dose and reaction time. *Biochar* 3:535–543. <https://doi.org/10.1007/s42773-021-00117-y>
- Liang QW, Luo HJ, Geng JJ, Chen JD (2018) Facile one-pot preparation of nitrogen-doped ultra-light graphene oxide aerogel and its prominent adsorption performance of Cr(VI). *Chem Eng J* 338:62–71. <https://doi.org/10.1016/j.cej.2017.12.145>
- Liang LP, Xi FF, Tan WS, Meng X, Hu BW, Wang XK (2021) Review of organic and inorganic pollutants removal by biochar and biochar-based composites. *Biochar* 3:255–281. <https://doi.org/10.1007/s42773-021-00101-6>
- Liao Y, Wang M, Chen DJ (2018) Preparation of polydopamine-modified graphene oxide/chitosan aerogel for uranium(VI) adsorption. *Ind Eng Chem Res* 57:8472–8483. <https://doi.org/10.1021/acs.iecr.8b01745>
- Liu WJ, Jiang H, Tian K, Ding YW, Yu HQ (2013) Mesoporous carbon stabilized MgO nanoparticles synthesized by pyrolysis of MgCl₂ preloaded waste biomass for highly efficient CO₂ capture. *Environ Sci Technol* 47(16):9397–9403. <https://doi.org/10.1021/es401286p>
- Liu LL, Luo XB, Ding L, Luo SL (2019) Application of nanotechnology in the removal of heavy metal from water. In: *Nanomaterials for the removal of pollutants and resource reutilization*. Elsevier, Amsterdam, pp 83–147
- Liu LQ, Huang YJ, Meng YH, Cao JH, Hu HJ, Su YH, Dong L, Tao SN, Ruan R (2020) Investigating the adsorption behavior and quantitative contribution of Pb²⁺ adsorption mechanisms on biochars by different feedstocks from a fluidized bed pyrolysis system. *Environ Res* 187:109609. <https://doi.org/10.1016/j.envres.2020.109609>
- Liu LF, Liu YL, Tan MM, Che NJ, Li CL (2021a) Double-network cross-linked aerogel with rigid and super-elastic conversion: simple formation, unique properties, and strong sorption of organic contaminants. *Environ Sci Pollut Res* 28:42637–42648. <https://doi.org/10.1007/s11356-021-13305-x>
- Liu PY, Rao D, Zou LY, Teng Y, Yu H (2021b) Capacity and potential mechanisms of Cd(II) adsorption from aqueous solution by blue algae-derived biochars. *Sci Total Environ* 767:145447. <https://doi.org/10.1016/j.scitotenv.2021.145447>
- Lu WH, Li JH, Sheng YQ, Zhang XS, You JM, Chen LX (2017) One-pot synthesis of magnetic iron oxide nanoparticle-multiwalled carbon nanotube composites for enhanced removal of Cr(VI) from aqueous solution. *J Colloid Interface Sci* 505:1134–1146. <https://doi.org/10.1016/j.jcis.2017.07.013>
- Lu L, Yu WT, Wang YF, Zhang K, Zhu XM, Zhang YC, Wu YJ, Ullah H, Xiao X, Chen BL (2020) Application of biochar-based materials in environmental remediation: from multi-level structures to specific devices. *Biochar* 2:1–2. <https://doi.org/10.1007/s42773-020-00041-7>
- Lu Y, Cai YW, Zhang S, Zhuang L, Hu BW, Wang SH, Chen JR, Wang XK (2022) Application of biochar-based photocatalysts for adsorption-(photo) degradation/reduction of environmental contaminants: mechanism, challenges and perspective. *Biochar* 4:45. <https://doi.org/10.1007/s42773-022-00173-y>
- Luo QY, Huang XH, Luo Y, Yuan HM, Ren TT, Li XJ, Xu D, Guo X, Wu YQ (2021) Fluorescent chitosan-based hydrogel incorporating titanate and cellulose nanofibers modified with carbon dots for adsorption and detection of Cr(VI). *Chem Eng J* 407:127050. <https://doi.org/10.1016/j.cej.2020.127050>
- Mei JF, Zhang H, Mo SQ, Zhang YZ, Li ZY, Ou HX (2020) Prominent adsorption of Cr(VI) with graphene oxide aerogel twined with creeper-like polymer based on chitosan oligosaccharide. *Carbohydr Polym* 247:116733. <https://doi.org/10.1016/j.carbpol.2020.116733>
- Mo YY, Wang SY, Vincent T, Desbrieres J, Faur C, Guibal E (2019) New highly-percolating alginate-PEI membranes for efficient recovery of chromium from aqueous solutions. *Carbohydr Polym* 225:115177. <https://doi.org/10.1016/j.carbpol.2019.115177>
- Mukherjee A, Zimmerman AR, Harris W (2011) Surface chemistry variations among a series of laboratory-produced biochars. *Geoderma* 163:247–255. <https://doi.org/10.1016/j.geoderma.2011.04.021>
- Neolaka YAB, Lawa Y, Naat JN, Riwu AAP, Iqbal M, Darmokoeseoemo H, Kusuma HS (2020) The adsorption of Cr(VI) from water samples using graphene oxide-magnetic (GO-Fe₃O₄) synthesized from natural cellulose-based graphite (kusambi wood or *Schleichera oleosa*): study of kinetics, isotherms and thermodynamics. *J Mater Res Technol* 9(3):6544–6556

- Neolaka YAB, Lawa Y, Naat J, Riwu AAP, Lindu YE, Darmokoeseomo H, Widyaningrum BA, Iqbal M, Kusuma HS (2021) Evaluation of magnetic material IIP@GO-Fe₃O₄ based on Kesambi wood (*Schleichera oleosa*) as a potential adsorbent for the removal of Cr(VI) from aqueous solutions. *React Funct Polym* 166:105000. <https://doi.org/10.1016/j.reactfunctpolym.2021.105000>
- Pang Y, Zeng GM, Tang L, Zhang Y, Liu YY, Lei XX, Li Z, Zhang JC, Xie GX (2011) PEI-grafted magnetic porous powder for highly effective adsorption of heavy metal ions. *Desalination* 281:278–284. <https://doi.org/10.1016/j.desal.2011.08.001>
- Peng SG, Liu CY, Fan XJ (2015) Surface modification of graphene oxide by carboxyl-group: preparation, characterization, and application for proteins immobilization. *Integr Ferroelectr* 163(1):42–53. <https://doi.org/10.1080/10584587.2015.1040328>
- Pradhan S, Abdelaal AH, Mroue K, Al-Ansari T, Mackey HR, McKa G (2020) Biochar from vegetable wastes: agro-environmental characterization. *Biochar* 2:439–453. <https://doi.org/10.1007/s42773-020-00069-9>
- Qiu MQ, Liu LJ, Ling Q, Cai YW, Yu SJ, Wang SQ, Fu D, Hu BW, Wang XK (2022) Biochar for the removal of contaminants from soil and water: a review. *Biochar* 4:19. <https://doi.org/10.1007/s42773-022-00146-1>
- Qu D, Zheng M, Du P, Zhou Y, Zhang LG, Li D, Tan HQ, Zhao Z, Xie ZG, Sun ZC (2013) Highly luminescent S, N co-doped graphene quantum dots with broad visible absorption bands for visible light photocatalysts. *Nanoscale* 5(24):12272–12277. <https://doi.org/10.1039/C3NR04402E>
- Rajapaksha AU, Alam MS, Chen N, Alessi DS, Igalavithana AD, Tsang DCW, Ok YS (2018) Removal of hexavalent chromium in aqueous solutions using biochar: chemical and spectroscopic investigations. *Sci Total Environ* 625:1567–1573. <https://doi.org/10.1016/j.scitotenv.2017.12.195>
- Sakhiya AK, Anand A, Kaushal P (2020) Production, activation, and applications of biochar in recent times. *Biochar* 2:253–285. <https://doi.org/10.1007/s42773-020-00047-1>
- Saleh TA, Tuzen M, Sari A (2018) Polyamide magnetic palygorskite for the simultaneous removal of Hg(II) and methyl mercury: with factorial design analysis. *J Environ Manag* 211:323–333. <https://doi.org/10.1016/j.jenvman.2018.01.050>
- Serrapede M, Rafique A, Fontana M, Zine A, Rivolo P, Bianco S, Chetibi L, Tresso E, Lamberti A (2019) Fiber-shaped asymmetric supercapacitor exploiting rGO/Fe₃O₄ aerogel and electrodeposited MnO_x nanosheets on carbon fibers. *Carbon* 144:91–100. <https://doi.org/10.1016/j.carbon.2018.12.002>
- Shaheen SM, Mosa A, Natasha AH, Niazi NK, Antoniadis V, Shahid M, Song H, Kwon EE, Rinklebe J (2022) Removal of toxic elements from aqueous environments using nano zero-valent iron- and iron oxide-modified biochar: a review. *Biochar* 4:24. <https://doi.org/10.1007/s42773-022-00149-y>
- Shang YX, Yang HQ, Qin Z, Yin SY, Yang LX, Xu MW, Li ZY, Jin ZQ, Sun H (2020) Arbitrary-shaped reduced graphene oxide aerogels via an unsaturated water vapor reduction. *Carbon* 168:169–179. <https://doi.org/10.1016/j.carbon.2020.06.080>
- Singh DK, Kumar V, Mohan S, Hasan SH (2017) Polylysine functionalized graphene aerogel for the enhanced removal of Cr(VI) through adsorption: kinetic, isotherm, and thermodynamic modeling of the process. *J Chem Eng Data* 62(5):1732–1742. <https://doi.org/10.1021/acs.jced.7b00188>
- Su QH, Su Z, Xie WY, Tian C, Su XT, Lin Z (2020) Preparation of 2D nitrogen-doped magnetic Fe₃C/C by in-situ self-assembled double-template method for enhanced removal of Cr(VI). *Environ Pollut* 263:114374. <https://doi.org/10.1016/j.envpol.2020.114374>
- Su QH, Khan AA, Su Z, Tian C, Li XQ, Gu JH, Zhang T, Ahmad R, Su XT, Lin Z (2021) Novel nitrogen-doped KFeS₂/C composites for the efficient removal of Cr(VI). *Environ Sci Nano* 8:1057. <https://doi.org/10.1039/d0en01283a>
- Sun C, Guo Y, Xu X, Du Q, Duan H, Chen Y, Li H, Liu H (2017) In situ preparation of carbon/Fe₃C composite nanofibers with excellent electromagnetic wave absorption properties. *Compos A* 92:33–41. <https://doi.org/10.1016/j.compositesa.2016.10.033>
- Tang Z, Kong YF, Zhao S, Jia HZ, Vione D, Kang YM, Gao P (2021) Enhancement of Cr(VI) decontamination by irradiated sludge biochar in neutral conditions: evidence of a possible role of persistent free radicals. *Sep Purif Technol* 277:119414. <https://doi.org/10.1016/j.seppur.2021.119414>
- Tran HN, You SJ, Hosseini-Bandegharaei A, Chao HP (2017) Mistakes and inconsistencies regarding adsorption of contaminants from aqueous solutions: a critical review. *Water Res* 120:88–116. <https://doi.org/10.1016/j.watres.2017.04.014>
- Vo AT, Nguyen VP, Ouakouak A, Nieva A, Doma BT Jr, Tran HN, Chao HP (2019) Efficient removal of Cr(VI) from water by biochar and activated carbon prepared through hydrothermal carbonization and pyrolysis: adsorption-coupled reduction mechanism. *Water* 11:1164. <https://doi.org/10.3390/w11061164>
- Wang H, Liu YG, Zeng GM, Hu XJ, Hu X, Li TT, Li HY, Wang YQ, Jiang LH (2014) Grafting of β-cyclodextrin to magnetic graphene oxide via ethylenediamine and application for Cr(VI) removal. *Carbohydr Polym* 113(113):166–173. <https://doi.org/10.1016/j.carbpol.2014.07.014>
- Wang H, Yuan XZ, Wu Y, Chen XH, Leng LJ, Wang H, Li H, Zeng GM (2015) Facile synthesis of polypyrrole decorated reduced graphene oxide-Fe₃O₄ magnetic composites and its application for the Cr(VI) removal. *Chem Eng J* 262:597–606. <https://doi.org/10.1016/j.cej.2014.10.020>
- Wang CC, Yang SD, Ma Q, Jia X, Ma PC (2017a) Preparation of carbon nanotubes/graphene hybrid aerogel and its application for the adsorption of organic compounds. *Carbon* 118:765–771. <https://doi.org/10.1016/j.carbon.2017.04.001>
- Wang DF, Zhang GL, Zhou LL, Wang M, Cai DQ, Wu ZY (2017b) Synthesis of a multifunctional graphene oxide-based magnetic nanocomposite for efficient removal of Cr(VI). *Langmuir* 33:7007–7014. <https://doi.org/10.1021/acs.langmuir.7b01293>
- Wang X, Liang YH, An WJ, Hu JS, Zhu YF, Cui WQ (2017c) Removal of chromium(VI) by a self-regenerating and metal free g-C₃N₄/graphene hydrogel system via the synergy of adsorption and photo-catalysis under visible light. *Appl Catal B* 219:53–62. <https://doi.org/10.1016/j.apcatb.2017.07.008>
- Wang XP, Lu J, Cao BY, Liu XM, Lin Z, Yang C, Wu RL, Su XT, Wang XF (2019) Facile synthesis of recycling Fe₃O₄/graphene adsorbents with potassium humate for Cr(VI) removal. *Colloid Surf A* 560:384–392. <https://doi.org/10.1016/j.colsurfa.2018.10.036>
- Wang X, Nie SB, Zhang P, Song L, Hu Y (2020) Superhydrophobic and superoleophilic graphene aerogel for ultrafast removal of hazardous organics from water. *J Mater Res Technol* 9(1):667–674. <https://doi.org/10.1016/j.jmrt.2019.11.008>
- Wang QY, Tian Y, Kong LC, Zhang J, Zuo W, Li YC, Cai GY (2021) A novel 3D superelastic polyethyleneimine functionalized chitosan aerogels for selective removal of Cr(VI) from aqueous solution: performance and mechanisms. *Chem Eng J* 425:131722. <https://doi.org/10.1016/j.cej.2021.131722>
- Wei C, Xiang C, Ren E, Cui C, Zhou M, Xiao HY, Jiang SX, Yao G, Shen H, Guo RH (2020) Synthesis of 3D lotus biochar/reduced graphene oxide aerogel as a green adsorbent for Cr(VI). *Mater Chem Phys* 253:123271. <https://doi.org/10.1016/j.matchemphys.2020.123271>
- White RL, White CM, Turgut H, Massoud A, Tian ZR (2018) Comparative studies on copper adsorption by graphene oxide and functionalized graphene oxide nanoparticles. *J Taiwan Inst Chem* 85:18–28. <https://doi.org/10.1016/j.jtice.2018.01.036>
- Xiao J, Hu R, Chen GC (2020) Micro-nano-engineered nitrogenous bone biochar developed with a ball-milling technique for high-efficiency removal of aquatic Cd(II), Cu(II) and Pb(II). *J Hazard Mater* 387:121980. <https://doi.org/10.1016/j.jhazmat.2019.121980>
- Xiong J, Zhou MG, Qu CC, Yu DH, Chen C, Wang MX, Tan WF (2021) Quantitative analysis of Pb adsorption on sulfhydryl-modified biochar. *Biochar* 3:37–49. <https://doi.org/10.1007/s42773-020-00077-9>
- Xu WH, Wang SF, Liu YG, Zeng GM, Zheng BH, Tan XF, Li TT, Wang H, Guo FY, Zhang MM (2015) Tartaric acid modified *Pleurotus ostreatus* for enhanced removal of Cr(VI) ions from aqueous solution: characteristics and mechanisms. *RSC Adv* 5(31):24009–24015. <https://doi.org/10.1039/C4RA17248E>
- Yang HS, Zhang TP, Jiang M, Duan YX, Zhang JM (2015) Ambient pressure dried graphene aerogels with superelasticity and multifunctionality. *J Mater Chem A* 3:19268–19272. <https://doi.org/10.1039/c5ta06452j>
- Yang YQ, Chen N, Feng CP, Li M, Gao Y (2018) Chromium removal using a magnetic corn cob biochar/polypyrrole composite by adsorption combined with reduction: reaction pathway and contribution degree. *Colloid Surf A* 556:201–209. <https://doi.org/10.1016/j.colsurfa.2018.08.035>
- Ye SB, Liu Y, Feng JC (2017) Low-density, mechanical compressible, water-induced self-recoverable graphene aerogels for water treatment. *ACS Appl Mater Interfaces* 9:22456–22464. <https://doi.org/10.1021/acsami.7b04536>
- Yu YT, Wu K, Xu WC, Chen DD, Fang JZ, Zhu XM, Sun JL, Liang Y, Hu XY, Li RQ, Fang ZQ (2020) Adsorption-photocatalysis synergistic removal of

- contaminants under antibiotic and Cr(VI) coexistence environment using non-metal g-C₃N₄ based nanomaterial obtained by supramolecular self-assembly method. *J Hazard Mater* 404:124171. <https://doi.org/10.1016/j.jhazmat.2020.124171>
- Yuan P, Wang J, Pan Y, Shen B, Wu C (2019) Review of biochar for the management of contaminated soil: preparation, application and prospect. *Sci Total Environ* 659:473–490. <https://doi.org/10.1016/j.scitotenv.2018.12.400>
- Zhang XP, Liu D, Yang L, Zhou L, You TY (2015) Self-assembled three-dimensional graphene-based materials for dye adsorption and catalysis. *J Mater Chem A* 3:10031–10037. <https://doi.org/10.1039/c5ta00355e>
- Zhang YY, Yan XR, Yan YY, Chen DJ, Huang LH, Zhang JX, Ke Y, Tan SZ (2018) The utilization of a three-dimensional reduced graphene oxide and montmorillonite composite aerogel as a multifunctional agent for wastewater treatment. *RSC Adv* 8(8):4239–4248. <https://doi.org/10.1039/c7ra13103h>
- Zhang LK, Mao JF, Chen BL (2019) Reconsideration of heterostructures of biochars: morphology, particle size, elemental position, reactivity and toxicity. *Environ Pollut* 254:113017. <https://doi.org/10.1016/j.envpol.2019.113017>
- Zhao J, Pan RJ, Sun R, Wen CY, Zhang SL, Wu B, Nyholm L, Zhang ZB (2019) High conductivity reduced-graphene-oxide/copper aerogel for energy storage. *Nano Energy* 60:760–767. <https://doi.org/10.1016/j.nanoen.2019.04.023>
- Zhitkovich A (2011) Chromium in drinking water: sources, metabolism, and cancer risks. *Chem Res Toxicol* 24(10):1617–1629. <https://doi.org/10.1021/tx200251t>
- Zhou L, Liu YG, Liu SB, Yin YC, Zeng GM, Tan XF, Hu X, Hu XJ, Jiang LH, Ding Y, Liu SH, Huang XX (2016) Investigation of the adsorption-reduction mechanisms of hexavalent chromium by ramie biochars of different pyrolytic temperatures. *Bioresour Technol* 218:351–359. <https://doi.org/10.1016/j.biortech.2016.06.102>
- Zou HW, Zhao JW, He F, Zhong Z, Huang JS, Zheng YL, Zhang Y, Yang YC, Yu F, Bashir MA, Gao B (2021) Ball milling biochar iron oxide composites for the removal of chromium (Cr(VI)) from water: performance and mechanisms. *J Hazard Mater* 413:125252. <https://doi.org/10.1016/j.jhazmat.2021.125252>

Submit your manuscript to a SpringerOpen[®] journal and benefit from:

- Convenient online submission
- Rigorous peer review
- Open access: articles freely available online
- High visibility within the field
- Retaining the copyright to your article

Submit your next manuscript at ► [springeropen.com](https://www.springeropen.com)
